Core-cancellation functions for evaluating exchange-correlation functionals in first-principles pseudopotential calculations

N. A. W. Holzwarth and Y. Zeng
Department of Physics, Wake Forest University, Winston-Salem, North Carolina 27109
(Received 21 May 1993; revised manuscript received 24 September 1993)

Within the framework of density-functional theory, first-principles pseudopotential methods have been highly successful in modeling the valence-electron properties of solids in their ground states. In this paper, we introduce "core-cancellation functions" which are designed to improve the accuracy of the treatment of the exchange-correlation interaction. This formalism, expected to be especially effective for transition metals, is tested for bulk tungsten and niobium, comparing results obtained using the local-density approximation to those obtained using the generalized gradient approximation.

I. INTRODUCTION

Density-functional theory[1] is based on the variational properties of the *total* electron density. However, for pedagogical and computational reasons, it is often necessary to divide the electron density into core and valence contributions. Kinetic energy and electrostatic interactions can easily be divided into core and valence terms. But for the exchange and correlation interactions, which are nonlinear functionals of the density, core and valence contributions are much harder to separate. Recently, Annett[2] has developed a density-functional theorem for the valence electrons alone, providing a rigorous framework for treating the core and valence electrons separately in the exchange and correlation interactions.[3,4] While these new ideas are being explored, it useful to improve techniques for accurately evaluating the well-established total electron density functionals.

First-principles pseudopotential techniques, which have been recently reviewed by Pickett[5] and Payne *et al.*,[6] enable a mathematically accurate method of separating core and valence interactions. In principle, a pseudopotential calculation can yield valence-electron energies and valence-electron densities in the bonding region arbitrarily close to that of an ideal full potential calculation in the frozen core approximation. Although the electrostatic contributions of the frozen core electrons are accurately represented, there has been some discussion of how to best include the effects of the frozen core electron density in the exchange and correlation interactions. Louie, Froyen, and Cohen[7] showed that since the frozen core density enters the exchange-correlation potential in a nonlinear functional form, it does not cancel out of the pseudopotential formulation. For transition metals, the effects of the core density in the exchange-correlation energy are magnified by the fact that the peak of the valence density occurs in a region of space where the core density is *an order of magnitude larger* than the valence density. This is demonstrated in Fig. 1, which contrasts the forms of the core and atomic valence densities for a covalent material *S*, with those of two transition metals, Nb and W, from the fourth and fifth rows of the Periodic Table. In their original paper, Louie, Froyen, and Cohen[7] showed that for most materials, it is sufficient to introduce a "partial core function" which is the exact core density in the region where there is large valence-core overlap, smoothly extended into the region close to the nucleus at a radius R_c by an approximate core density function. For Fe, Zhu, Wang, and Louie[8] report that results are sensitive functions of the cutoff radius R_c. We found that for W and other transition metals we could not reliably calculate the electronic structure using the partial core functions, and therefore adopted a full core density treatment of these effects with the help of "core-cancellation functions." This treatment is a modification of an idea originally presented by Bylander and Kleinman,[9] and may be especially convenient for pseudopotential inversion calculations.[10] It improves the numerical accuracy of the evaluation of exchange and correlation contributions to the cohesive energy of the system and we are able to compare the results calculated with the local density approximation[11] (LDA) with those obtained using the new generalized gradient approximation (GGA-II), recently developed by Perdew *et al.*[12]

The outline of this paper is as follows. In Sec. II, the mathematical formalism and computational details are presented, including an outline of the complete cohesive energy calculation and a description of the core-calculation formalism. In Sec. III, results for bulk W are presented, comparing the results obtained with the LDA and GGA-II forms of the density functional with those of previous workers. Discussion and conclusions are given in Sec. IV.

II. COMPUTATIONAL METHODS

A. Outline of cohesive energy calculation

The computation techniques used in this study are based on density-functional theory, within the frozen core approximation, implemented using norm-conserving pseudopotentials and a mixed-basis representation of the electronic wave functions, as outlined in the original work of Louie, Ho, and Cohen.[13] The basic calculational

scheme used in this work is very similar to that used by many groups as reviewed by Pickett[5] and by Payne *et al.*[6] However, as calculations are pushed to greater accuracy, details of the computational techniques become important.

In the first step of the calculation, the norm-conserving pseudopotentials are constructed from a self-consistent solution of the Dirac equation for the atom by the method of Kleinman[14] and Bachelet, Hamann, and Schlüter.[15] In our work, we use the functional form of Kerker[16] and some of the modifications suggested by Troullier and Martins[17] in order to increase the smoothness of the pseudopotential. From the spin averaged pseudopotentials of the neutron atom $V_l^{\rm atom}(r)$, the ionic pseudopotentials $V_l^{\rm ion}(r)$ are determined by subtracting the valence screening potential $V^{\rm screen}(\rho_{\rm core}^{\rm atom},\rho^{\rm atom})$ which, as defined below, is a function of the frozen core density $\rho_{\rm core}^{\rm atom}$ and the valence pseudodensity $\rho^{\rm atom}$:

$$V_l^{\rm ion}(r)=V_l^{\rm atom}(r)-V^{\rm screen}(\rho_{\rm core}^{\rm atom},\rho^{\rm atom}) . \quad (1)$$

In general, the complete ionic pseudopotential can be conveniently divided into local and nonlocal terms[5,6,13]:

$$V^{\rm ion}(r)=V_{\rm local}^{\rm ion}(r)+\delta V_l^{\rm ion}(r)\mathcal{P}_l , \quad (2)$$

where $\mathcal{P}_l$ is the projection operator for angular momentum about the ion center and where

$$\delta V_l^{\rm ion}(r)\equiv V_l^{\rm ion}(r)-V_{\rm local}^{\rm ion}(r) .$$

It is mathematically accurate and computationally convenient to choose:

$$V_{\rm local}^{\rm ion}(r)=V_{l_{\rm max}}^{\rm ion}(r) , \quad (3)$$

where $l_{\rm max}$ is the largest angular momentum of the valence electrons. In this way, errors in the matrix elements from high angular momentum partial waves can be made as small as possible and also the nonlocal terms $\delta V_l^{\rm ion}(r)\mathcal{P}_l$ must be calculated for the fewest number of terms; $l<l_{\rm max}$. In the present work, spin-orbit interactions[14,15] were not included.

With a knowledge of the ionic pseudopotentials, for a given geometry of the ionic coordinates $\{\tau\}$, and for an initial guess of the valence-electron density $\rho^{\rm in}$, the effective Hamiltonian of the density-functional equations[1] can be constructed. The valence-electron density enters the effective Hamiltonian in terms of the screening potential $V^{\rm screen}(\rho_{\rm core},\rho^{\rm in})$ which represents the Coulomb repulsion and exchange-correlation interaction of the valence electrons and has the same functional form as in the atomic calculation [Eq. (1)], but now $\rho_{\rm core}$ represents the superposition of all of the (possibly overlapping) frozen core densities of the ions in the solid and $\rho^{\rm in}$ represents the valence pseudodensity of the solid.

For each wave vector $\mathbf{k}$, it is assumed that the valence eigenfunctions can be accurately represented with the following mixed-basis expansion[13]:

$$\Psi_{N\mathbf{k}}(\mathbf{r})=\sum_G \alpha_N^{\rm G}(\mathbf{k})e^{i(\mathbf{k}+\mathbf{G})\cdot\mathbf{r}}+\sum_\mu \beta_N^\mu(\mathbf{k})\Phi^\mu(\mathbf{k},\mathbf{r}) . \quad (4)$$

In this expansion, $\mathbf{G}$ denotes a reciprocal lattice vector of the plane wave function and $\Phi^\mu(\mathbf{k},\mathbf{r})$ denotes a linear-combination-of-atomic-orbital (LCAO) function with μ representing the site and orbital-type index. The LCAO basis functions are formed from the atomic pseudo wave functions and are typically chosen to represent only the highly localized contributions such as d-wave terms for transition metals and s- and p-wave terms for materials in the first few rows of the Periodic Table. The number of plane-wave terms is controlled through the parameter $q_{\rm PW}$ by including all terms such that $|\mathbf{k}+\mathbf{G}|\le q_{\rm PW}$. These represent delocalized wave-function contributions as well as shape changes to the atomic LCAO basis func-

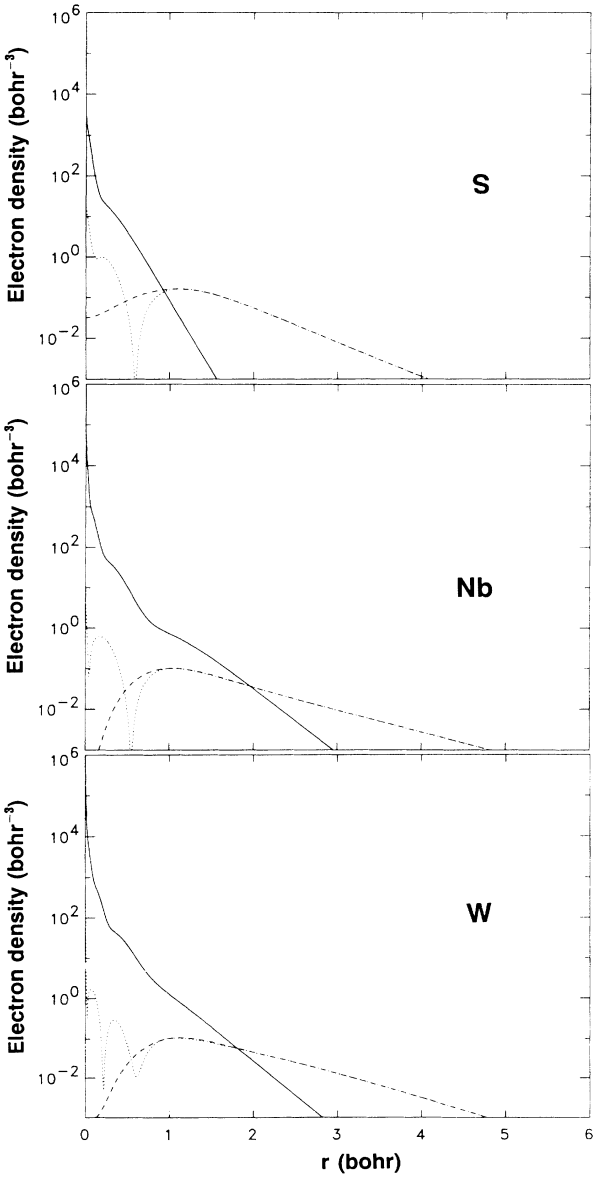

FIG. 1. Core and valence-electron densities for S, Nb, and W atoms evaluated with the GGA-II form of the exchange-correlation interaction. For each atom, the core electron density is indicated with a solid line, the full potential valence-electron density is indicated with a dotted line, and the pseudopotential valence-electron density is indicated with a dashed line.

tions caused by interactions in the solid. In evaluating the matrix elements of the Kohn-Sham equations,[1] the LCAO contributions are evaluated by using plane-wave expansions including all $|\mathbf{k}+\mathbf{G}| \leq q_{\mathrm{LCAO}}$. The number of LCAO basis functions and the convergence parameters q_{PW} and q_{LCAO} are chosen so that the mixed-basis set is well converged but not overcomplete. The matrix elements of the local potential contributions are evaluated by using fast Fourier transform (FFT) techniques,[13] with a maximum reciprocal lattice vector $Q_{\max}$ (which must be larger than q_{PW} and q_{LCAO}) chosen to accurately compute the FFT of the valence density, the valence screening potential, and the local ionic pseudopotentials. The matrix elements of the nonlocal potential contributions are evaluated by a separable form approximation.[18] The wave-function coefficients $\alpha_N^G(\mathbf{k})$ for the plane-wave contributions and $\beta_N^\mu(\mathbf{k})$ for the LCAO contributions are determined by solving a generalized eigenvalue problem of the form

$$(\mathsf{H}-E_{N\mathbf{k}}\mathsf{S})\Lambda_{N\mathbf{k}}=0, \quad \Lambda_{N\mathbf{k}}=\begin{bmatrix}\alpha\\ \beta\end{bmatrix}, \tag{5}$$

where H represents the Hamiltonian matrix and S represents the overlap matrix. Here $E_{N\mathbf{k}}$ denotes the one-electron eigenvalue corresponding to the eigenstate $\Psi_{N\mathbf{k}}$. The dimension of the generalized eigenvalue problem (5) is generally 500–2000 for materials we have studied. Eigenvalues for the occupied states and a few unoccupied states were determined with standard diagonalization[19] methods.

From a knowledge of the eigenstates, the resulting valence electron pseudodensity can be determined:

$$\rho^{\mathrm{out}}(r)=\sum_{N\mathbf{k}} w_{N\mathbf{k}}|\Psi_{N\mathbf{k}}(r)|^2 . \tag{6}$$

Here, integration over the Brillouin zone is approximated by a midpoint sampling on a uniform grid, using symmetry considerations to determine the number irreducible $\mathbf{k}$ points and their fractional degeneracies $d_{\mathbf{k}}$. This $\mathbf{k}$-point sampling is the same as that used for calculating the density of states as developed by Gilat and Kam[20] and works as well for metals as it does for semiconductors and insulators. We investigated several methods of determining the weighted occupancies $w_{N\mathbf{k}}$, finding the method of Fu and Ho[21] to give the best results:

$$w_{N\mathbf{k}}=d_{\mathbf{k}}\left[1+\mathrm{erf}\left[\frac{E_F-E_{N\mathbf{k}}}{\sigma}\right]\right], \tag{7}$$

where it is assumed that $\sum_{\mathbf{k}} d_{\mathbf{k}}=1$ and that there is double occupancy for each full band state. Here, σ represents a Gaussian width associated with each band which should be chosen to approximate the dispersion between adjacent grid points. The results are insensitive to the choice of σ.[21] The Fermi level is determined by solving the transcendental equation:

$$\sum_{N\mathbf{k}} w_{N\mathbf{k}}=N_{\mathrm{total}} , \tag{8}$$

where N_{total} represents the total number of valence electrons in the unit cell. This procedure effectively stabilizes the density iterations.

Once the output density has been calculated [Eq. (6)], the convergence of the density is checked by testing whether the following inequality is satisfied:

$$\sum_{\mathbf{G}} |\rho^{\mathrm{out}}(\mathbf{G})-\rho^{\mathrm{in}}(\mathbf{G})| \leq \Delta_\rho , \tag{9}$$

where Δ_ρ is the density convergence parameter set for the calculation. If the valence density has not yet converged, a new input density is generated using the Broyden[22] algorithm as implemented by Srivastava[23] and the Kohn-Sham calculation is repeated.

If the valence-electron pseudodensity has converged, then $\rho^{\mathrm{out}} \approx \rho^{\mathrm{in}} \equiv \rho$, and the cohesive energy $E_{\mathrm{coh}}(\{\tau\})$ can be calculated for the given ionic coordinates $\{\tau\}$ from the following six contributions:

$$E_{\mathrm{coh}}=E_{\mathrm{atom}}-(E_{\mathrm{Ewald}}+E_{\mathrm{one}}+E_{\mathrm{Coul}}+E_{\mathrm{xc}}+E_{\mathrm{ck}}) . \tag{10}$$

The last five terms represent the valence electron energy of the solid which is subtracted from the valence-electron energy of the free ground-state atoms, E_{atom}, to determine the cohesive energy of the material. The term E_{Ewald} denotes the ion-ion interaction screened by a uniform distribution of compensating negative charge, evaluated using an Ewald summation.[24] The term E_{one},

$$E_{\mathrm{one}}=\sum_{N\mathbf{k}} w_{N\mathbf{k}}E_{N\mathbf{k}} , \tag{11}$$

is the weighted sum of the one-electron eigenvalues $E_{N\mathbf{k}}$ of the Hamiltonian (5). In this work, the "zero" for the one-electron eigenvalues is fixed by choosing the $\mathbf{G}=0$ Fourier transform of each local ionic pseudopotentials to be[25]

$$\tilde{V}_{\mathrm{local}}^{\mathrm{ion}}(\mathbf{G}=0)=\frac{4\pi}{\Omega}\int r^2 dr\left[V_{\mathrm{local}}^{\mathrm{ion}}(r)+\frac{Ze^2}{r}\right], \tag{12}$$

where Ω denotes the volume of the unit cell and where Z denotes the valence charge of the ion. The term E_{Coul},

$$E_{\mathrm{Coul}}=-\frac{e^2}{2}\int d^3r\, d^3r'\frac{[\rho(r)-\rho_0][\rho(r')-\rho_0]}{|r-r'|} , \tag{13}$$

is the electron-electron repulsion correction to E_{one}, from which a uniform distribution of compensating charge $\rho_0 \equiv N_{\mathrm{total}}/\Omega$ is subtracted. The formulation of the norm-conserving pseudopotentials ensures that these three terms $(E_{\mathrm{Ewald}}+E_{\mathrm{one}}+E_{\mathrm{Coul}})$ are determined accurately, provided that the canceling divergences in the $G=0$ contributions are treated properly.[25] The term E_{xc} represents the exchange-correlation contributions and is described in detail in Sec. II B below. The term E_{ck} represents a very small correction for core electron repulsion which is also described in Sec. II B below. The atomic valence energies in E_{atom} are calculated using the same pseudopotentials as used in the solid calculations so that there is significant error cancellation in determining the cohesive energy. However, there is a systematic error caused by the fact that in the atomic program, the atomic valence energies are calculated for spherically averaged valence densities, corresponding to the multiplet average of the atomic ground-state configurations. However, the

experimental cohesive energy is based on the true atomic ground-state multiplets which can be lower than the multiplet averages by as much as a few electron volts for each atom. A reasonable estimate of the multiplet average energy relative to the atomic ground state can be determined for each atom from the experimental spectroscopic levels listed in the Moore tables.[26] The sum of these multiplet averages can be used to calculate an atomic multiplet correction $\Delta E_{\rm atom}^{\rm mult}$ which can then be used to correct the cohesive energy[27]:

$$E_{\rm coh}^{\rm corr} \equiv E_{\rm coh} - \Delta E_{\rm atom}^{\rm mult} \ . \tag{14}$$

Since $\Delta E_{\rm atom}^{\rm mult}$ is a positive energy, this correction reduces the magnitude of the cohesive energy.

So far, we have used this method to study systems with relatively few degrees of freedom so that it has been convenient to determine the highest cohesive energy $E_{\rm max}$ by sampling $E_{\rm coh}(\{\tau\})$ on a grid of possible geometries, using interpolation to estimate the maximum. In evaluating $E_{\rm coh}(\{\tau\})$ at adjacent geometries, it is often advantageous to start the density iterations by using the initial valence pseudodensity $\rho^{\rm in}$ obtained by evaluating Eq. (6), using the occupancies $w_{N\mathbf{k}}$ and the wave-function coefficients $\alpha_N^G(\mathbf{k})$ and $\beta_N^\mu(\mathbf{k})$ from the results of a nearby geometry, but adjusting the LCAO basis functions $\Phi^\mu(\mathbf{k},\mathbf{r})$ to the correct geometry. This procedure usually substantially reduces the number of iterations needed to converge the density. The completed calculation yields the maximum cohesive energy geometry in terms of the ionic coordinates $\{\tau\}$, the corresponding self-consistent valence-electron pseudodensity $\rho^{\rm out} \approx \rho^{\rm in} \equiv \rho$ and cohesive energy $E_{\rm coh}^{\rm corr}$, and the corresponding one-electron eigenstates $\Psi_{N\mathbf{k}}(\mathbf{r})$ and eigenenergies $E_{N\mathbf{k}}$.

The methods described above are very similar to those discussed in the literature.[5,6] The new core-cancellation functions for the exchange-correlation interaction described in Sec. II B below affects the creation of the pseudopotential functions, the evaluation of the valence screening interaction $V^{\rm screen}$, and the evaluation of the exchange-correlation contribution to the cohesive energy $E_{\rm xc}$.

B. Core-cancellation functions for evaluating exchange-correlation functionals

For a given valence pseudodensity function $\rho(\mathbf{r})$ and frozen core density function $\rho_{\rm core}(\mathbf{r})$, we can define the valence screening potential in terms of Coulomb repulsion and exchange-correlation contributions:

$$V^{\rm screen}(\rho_{\rm core},\rho) = e^2 \int d^3r' \frac{\rho(\mathbf{r}')}{|\mathbf{r}-\mathbf{r}'|} + \{ V_{\rm xc}[\rho_{\rm core}(\mathbf{r})+\rho(\mathbf{r})] - V_{\rm xc}^{\rm core}(\mathbf{r}) \} \ . \tag{15}$$

For calculations in solids, $\rho(\mathbf{r}')$ is replaced by $[\rho(\mathbf{r}')-\rho_0]$ in the Coulomb repulsion term. The corresponding exchange-correlation energy used in Eq. (10) can be written

$$E_{xc} \equiv \int d^3r \{ \mathcal{E}_{\rm xc}(\rho_{\rm core}(\mathbf{r}),\rho(\mathbf{r})) - \mathcal{E}_{\rm xc}^{\rm core}(\mathbf{r}) \} \ , \tag{16}$$

where the exchange energy density function is defined by

$$\mathcal{E}_{\rm xc}[\rho_{\rm core}(\mathbf{r}),\rho(\mathbf{r})] \equiv [\rho_{\rm core}(\mathbf{r})+\rho(\mathbf{r})]\epsilon_{\rm xc}[\rho_{\rm core}(\mathbf{r})+\rho(\mathbf{r})] - \rho(\mathbf{r}) V_{\rm xc}[\rho_{\rm core}(\mathbf{r})+\rho(\mathbf{r})] \ . \tag{17}$$

In Eqs. (15) and (17), the standard notation[1] for the exchange-correlation functionals $\epsilon_{\rm xc}(n)$ and

$$V_{\rm xc}(n) \equiv \frac{\delta[n\epsilon_{\rm xc}(n)]}{\delta n}$$

is used. In the present work, we have used both the exchange-correlation functional forms of Ceperley and Alder[28] as parametrized by Perdew and Wang[11] for the LDA and of Perdew *et al.*[12] for the GGA-II calculations. We have restricted our calculations to zero spin polarization, but generalization to include the possibility of spin polarization is straightforward. For the LDA calculations, relativistic corrections for the uniform electron gas, as calculated by MacDonald and Vosko[29] and Rajagopal[30] were added to the nonrelativistic contributions.

The core-cancellation functions $V_{\rm xc}^{\rm core}(\mathbf{r})$ and $\mathcal{E}_{\rm xc}^{\rm core}(\mathbf{r})$ are added to Eqs. (15) and (16) in order to increase the efficiency and accuracy of the calculation. These functions are chosen to serve two purposes: (a) to ensure that the net exchange-correlation functions that are used in the calculation [the terms in the curly brackets of Eqs. (15) and (16)] are *smooth* and (b) to have *no residual effects* on the calculation. Criterion (a) is fulfilled by choosing the cancellation functions so that they *cancel* the rapid varying behavior of $V_{\rm xc}[\rho_{\rm core}(\mathbf{r})+\rho(\mathbf{r})]$ and of $\mathcal{E}_{\rm xc}(\rho_{\rm core}(\mathbf{r}),\rho(\mathbf{r}))$ near each ion site, as suggested in the original paper of Bylander and Kleinman.[9] Criterion (b) is fulfilled by constructing $V_{\rm xc}^{\rm core}(\mathbf{r})$ and $\mathcal{E}_{\rm xc}^{\rm core}(\mathbf{r})$ from *nonoverlapping* atomic contributions. $V_{\rm xc}^{\rm core}(\mathbf{r})$ enters the calculation in constructing the ionic pseudopotentials [Eq. (1)] by subtracting $V^{\rm screen}$ from the neutral atomic pseudopotential. It also enters the calculation in constructing the Hamiltonian for the solid by adding $V^{\rm screen}$ for the solid to the other Hamiltonian contributions. Since $V_{\rm xc}^{\rm core}(\mathbf{r})$ enters both of these contributions with identical value and opposite sign, it cancels out of the net calculation. $\mathcal{E}_{\rm xc}^{\rm core}(\mathbf{r})$ enters the calculation of the atomic valence energy through the exchange-correlation energy [Eq. (16)] evaluated for the valence density of the atom, $\rho^{\rm atom}$, and also enters the calculation of the valence-electron energy of the solid through the exchange-correlation energy [Eq. (16)] evaluated for the valence density of the solid, ρ. $\mathcal{E}_{\rm xc}^{\rm core}(\mathbf{r})$ enters both of these contributions identically and with opposite sign in the calculation of the cohesive energy [Eq. (10)] and thus cancels out of the net calculation.

Within criteria (a) and (b), there is considerable flexibility in the choice of form for the radial functions $V_{\rm xc}^{\rm core}(r)$ and $\mathcal{E}_{\rm xc}^{\rm core}(r)$, centered at each ion site, that compose the complete cancellation functions for the solid. We have used the following two choices for the functional forms:

$$V_{\rm xc}^{\rm core}(r) \equiv V_{\rm xc}[\tilde{\rho}_{\rm core}^{\rm atom}(r)] \ ,$$

$$\mathcal{E}_{\rm xc}^{\rm core}(r) \equiv \tilde{\rho}_{\rm core}^{\rm atom}(r)\epsilon_{\rm xc}[\tilde{\rho}_{\rm core}^{\rm atom}(r)] \ ,$$

where

$$\tilde{\rho}_{\rm core}^{\rm atom}(r)\equiv\rho_{\rm core}^{\rm atom}(r)f_{\rm cut}(r)\ , \tag{18a}$$

or

$$V_{\rm xc}^{\rm core}(r)\equiv V_{\rm xc}[\rho_{\rm core}^{\rm atom}(r)+\rho^{\rm atom}(r)]f_{\rm cut}(r)\ ,$$
$$\mathcal{E}_{\rm xc}^{\rm core}(r)\equiv\mathcal{E}_{\rm xc}(\rho_{\rm core}^{\rm atom}(r),\rho^{\rm atom}(r))f_{\rm cut}(r)\ . \tag{18b}$$

In these equations, the notation $\rho_{\rm core}^{\rm atom}(r)$ is used to denote the spherically symmetric frozen core density of a single atom, while $\rho_{\rm core}(\mathbf{r})$ used in Eqs. (15)–(17) denotes the superposition of all of the (possibly overlapping) frozen core densities in the solid. Both forms (18a) and (18b) use a cutoff function which vanishes outside a sphere of radius r_c about the atom. The cutoff radius r_c is chosen so that there is no overlap of the cancellation functions for any of the solid geometries considered in the calculations. Typically, the cutoff radius r_c is chosen to be the largest of the radii used to construct the corresponding ionic pseudopotential. In this work, we have chosen the cutoff function to have the form:

$$f_{\rm cut}(r)=e^{-(1.5\cdot r/r_c)^8}\ . \tag{19}$$

We found form (18a) to work well for the LDA calculations. However, for the generalized gradient approximation, which depends on the gradient of the density, the use of the cutoff function within the exchange-correlation functionals caused unphysical structure in the cancellation functions. We found the choice of functional form indicated in Eq. (18b) to work well with the GGA-II exchange-correlation functional and expect it to also work well for the LDA.

While the presence of the cutoff function ensures that the cancellation functions will be nonoverlapping, it is important to check the behavior of the net exchange-correlation functionals at each ion center, as $r\rightarrow 0$. Since in this region, the core electron density dominates, $\rho_{\rm core}\gg\rho$, when $V_{\rm xc}$ and $\epsilon_{\rm xc}$ are functionals of the density only (LDA) it is possible to make a Taylor's series analysis yielding the following asymptotic form corresponding to (18a):

$$V_{\rm xc}(\rho_{\rm core}+\rho)-V_{\rm xc}^{\rm core}\underset{(r\rightarrow 0)}{\approx}V'_{\rm xc}(\tilde{\rho}_{\rm core}^{\rm atom})(\rho+\delta\rho_{\rm core})\ ,$$
$$\mathcal{E}_{\rm xc}(\rho_{\rm core},\rho)-\mathcal{E}_{\rm xc}^{\rm core}\underset{(r\rightarrow 0)}{\approx}V_{\rm xc}(\tilde{\rho}_{\rm core}^{\rm atom})\delta\rho_{\rm core} \tag{20a}$$
$$-\tfrac{1}{2}V'_{\rm xc}(\tilde{\rho}_{\rm core}^{\rm atom})(\rho^2-\delta\rho_{\rm core}^2)\ ,$$

where $\delta\rho_{\rm core}$ denotes $\rho_{\rm core}-\tilde{\rho}_{\rm core}^{\rm atom}$ and $V'_{\rm xc}(n)$ denotes the derivative $dV_{\rm xc}(n)/dn$. The asymptotic form corresponding to (18b) is given by

$$V_{\rm xc}(\rho_{\rm core}+\rho)-V_{\rm xc}^{\rm core}\underset{(r\rightarrow 0)}{\approx}V_{\rm xc}(\rho_{\rm core}+\rho)(1-f_{\rm cut})+V'_{\rm xc}(\rho_{\rm core}^{\rm atom}+\rho^{\rm atom})(\rho_{\rm core}-\rho_{\rm core}^{\rm atom}+\rho-\rho^{\rm atom})f_{\rm cut}\ ,$$
$$\mathcal{E}_{\rm xc}(\rho_{\rm core}+\rho)-\mathcal{E}_{\rm xc}^{\rm core}\underset{(r\rightarrow 0)}{\approx}\mathcal{E}_{\rm xc}(\rho_{\rm core},\rho)(1-f_{\rm cut})+\{V_{\rm xc}(\rho_{\rm core}^{\rm atom}+\rho^{\rm atom})(\rho_{\rm core}-\rho_{\rm core}^{\rm atom}) \tag{20b}$$
$$+\tfrac{1}{2}V'_{\rm xc}(\rho_{\rm core}^{\rm atom}+\rho^{\rm atom})[(\rho_{\rm core}-\rho_{\rm core}^{\rm atom}-\rho^{\rm atom})^2-\rho^2]\}f_{\rm cut}\ .$$

As $r\rightarrow 0$, it is apparent that $f_{\rm cut}\approx 1$ and that $\rho_{\rm core}\approx\rho_{\rm core}^{\rm atom}$. For the LDA formulation, it can be shown that $V'_{\rm xc}(n)$ vanishes for large n so that all of these net exchange-correlation functions go smoothly to zero as $r\rightarrow 0$. For the GGA-II formulation, there are additional terms in the Taylor's series expansion due to the dependence of $\epsilon_{\rm xc}$ on the gradient of the density. However, it can be shown that these additional terms which should be added to Eq. (20b) also smoothly vanish as $r\rightarrow 0$. Thus, it is apparent that the net exchange-correlation potentials and energy densities go smoothly to zero near each ion nucleus as designed. Figures 2 and 3 show the net exchange-correlation functionals for S, Nb, and W and their corresponding ionic pseudopotentials. In each of these cases, the net exchange-correlation functionals are clearly shown to be smooth everywhere and to smoothly vanish as $r\rightarrow 0$ as argued above. The net exchange-correlation potential has a maximum magnitude of less than 10% of the maximum magnitude of the corresponding ionic pseudopotential and the net exchange-correlation energy density is an order of magnitude smaller.

Since the smooth form of the net exchange-correlation functionals relies on the largeness of the core density relative to that of the valence density and not on its shape, it is clear why that a similar analysis would apply to the approximate core formulation of Louie, Froyen, and Cohen,[7] explaining why it generally works well. One advantage of the present formulation is that it takes better numerical advantage of the cancellation of terms. From Figs. 2 and 3, it is clear the net exchange-correlation density function is numerically much smaller than its individual contributions. In most of the materials that we have studied so far, we find that $E_{\rm xc}$ has a magnitude of less than 15% of $E_{\rm coh}$; for Nb and W it is less than 5%, several times smaller than its magnitude calculated using the partial core correction.[7] In addition to the numerical advantage of the present formulation, it also improves the accuracy of the pseudopotential approximation relative to the full potential treatment, since it can be shown that the full potential and pseudopotential values of the net exchange-correlation energy density function are very similar except for a small volume close to the nuclei.

The net exchange-correlation functionals which enter the electronic structure calculations are thus demonstrated to be spatially smooth functions. In calculations for periodic solids, these terms are most conveniently evaluated on the real-space fast-Fourier-transform (FFT) grid[13] used to evaluate the valence-electron density. Since the core density is spatially well localized, it can easily be evaluated directly on the real-space grid without

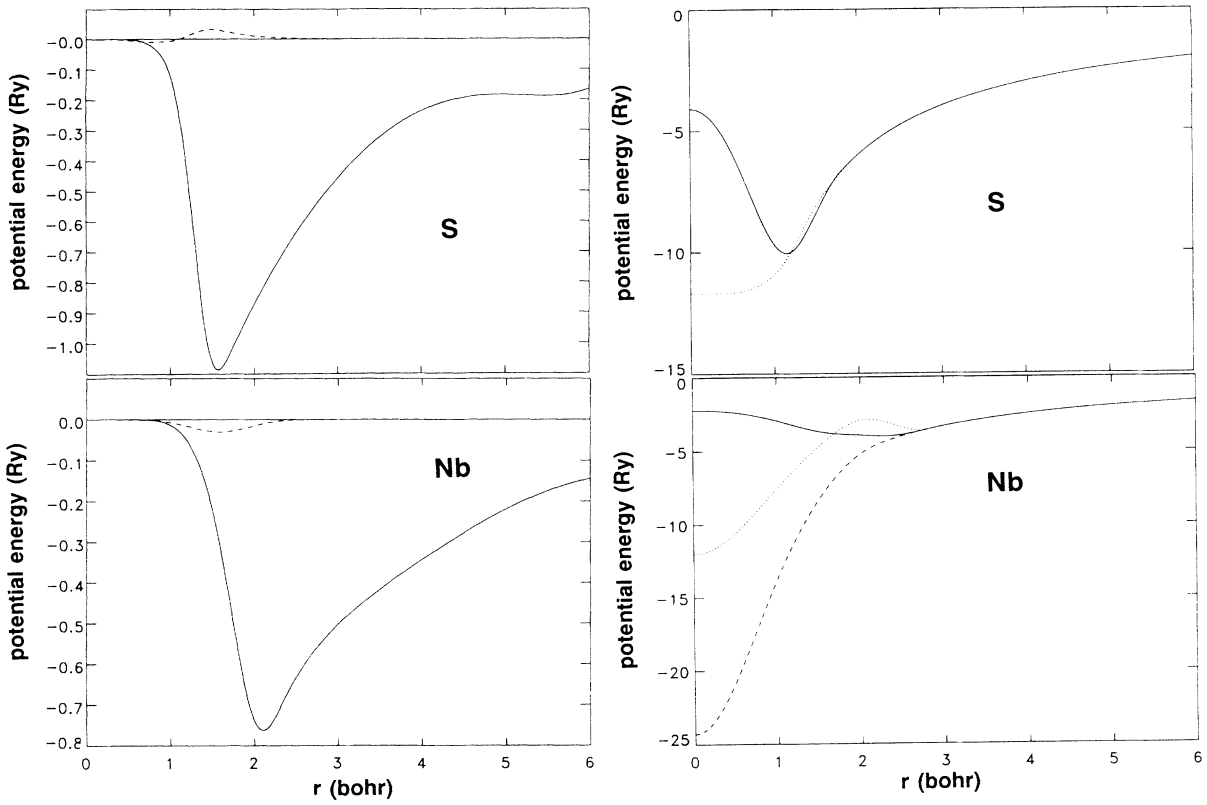

FIG. 2. Potentials for S and Nb evaluated using the GGA-II form of the exchange-correlation interaction with the core-cancellation function given by Eq. (18b). Left panels show net exchange-correlation potentials (solid line) and net exchange-correlation energy densities (dashed line). Right panels show corresponding pseudopotentials for $l=0$ (solid line), $l=1$ (dotted line), and $l=2$ (dashed line).

having to evaluate its Fourier transforms. For the GGA-II formulation, the first and second derivatives of the core density must also be evaluated on the real-space grid. Since the core density is fixed, its evaluation on the FFT grid and that of its derivatives can be stored throughout the self-consistency loop.

In the case of W, the core states are unusually extended such that they overlap each other slightly in crystalline W at the equilibrium lattice geometry.[31] The core cancellation function treatment of the exchange correlation interaction as described above, correctly treats the effects of this core overlap in the frozen core approximation. The Coulomb interactions are also well approximated through the overlapping ionic pseudopotentials. Both of these terms estimate the additional attractive forces in the system due to overlapping core electrons. The repulsive effects of the overlapping core electrons have been completely omitted in this formulation. In an attempt to account for the repulsive effects, we have added an additional term to the total energy of the system, Eq. (10), in the form of a Thomas-Fermi treatment of the overlapping core kinetic energy:

$$E_{\rm ck}\equiv\frac{3}{10}\frac{\hbar^2}{m}(3\pi^2)^{2/3}\int d^3r\left[\left[\sum_\tau \rho_{\rm core}(\mathbf{r}-\tau)\right]^{5/3}-\sum_\tau[\rho_{\rm core}(\mathbf{r}-\tau)]^{5/3}\right], \quad (21)$$

where the sums over τ indicate summations over all lattice sites. The first term approximates the total kinetic-energy contribution of the overlapping frozen core electrons in the solid, while the second term subtracts the corresponding atomic frozen core kinetic-energy contributions. This energy can be evaluated on the same FFT grid as for the exchange-correlation contribution, although care must be taken to properly evaluate the divergences near each nucleus. This contribution is identically zero for nonoverlapping cores and represents a very small repulsive interaction between nuclei even for W (less than 1% of $E_{\rm coh}$ at equilibrium). In retrospect, the core kinetic-energy correction term $E_{\rm ck}$ can be safely omitted from most calculations.

III. TEST RESULTS FOR BULK Nb AND W

The convergence and tolerance parameters $Q_{\rm max}$, $q_{\rm PW}$, $q_{\rm LCAO}$, and Δ_ρ used to study the ground-state properties of Nb W are summarized in Table I for both the LDA and GGA-II calculations. The pseudopotential radii used to construct the pseudopotentials shown in Figs. 2 and 3 are also listed in this table. These parameters were chosen so that the GGA-II calculation for W was very well converged. The LDA calculation for W and the calculations for Nb converged at smaller values of the cutoff parameters.

For W, calculations were performed assuming the bcc

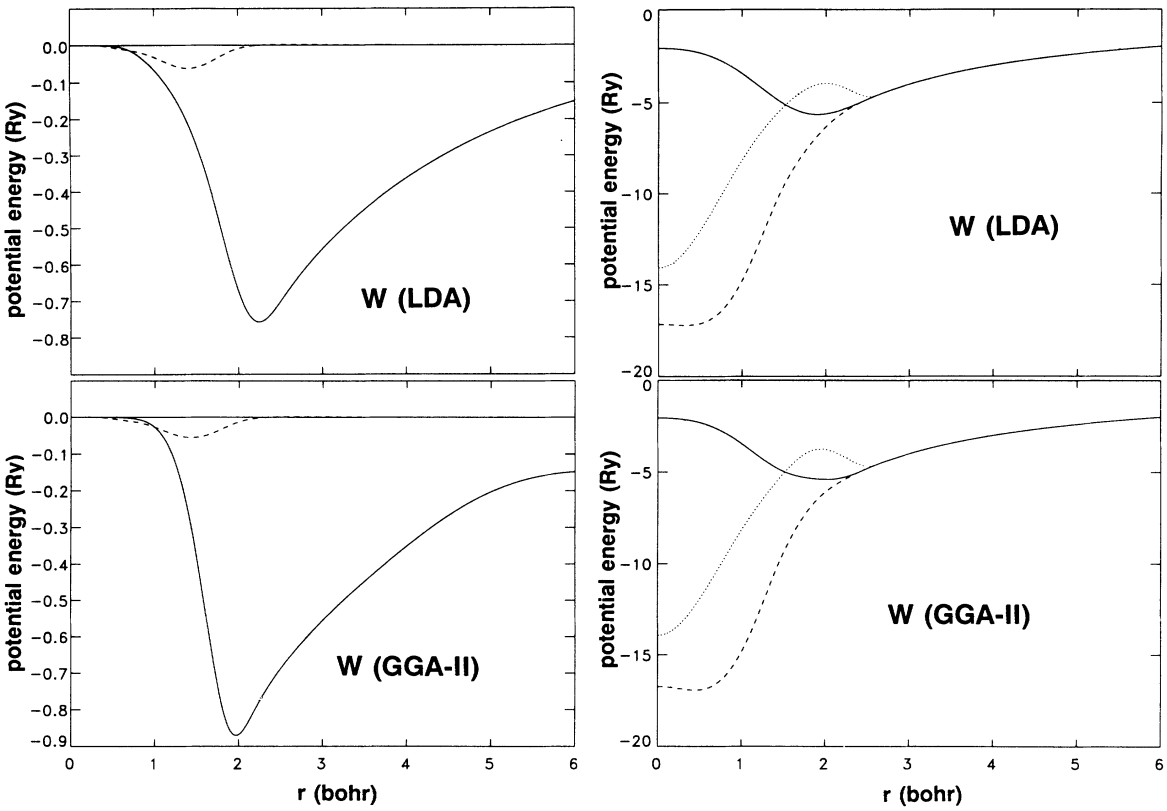

FIG. 3. Potentials for W evaluated using the LDA form of the exchange-correlation interaction with the core-cancellation function given by Eq. (18a) (top panels) and using the GGA-II form of the exchange-correlation interaction with the core-cancellation function given by Eq. (18b) (bottom panels). Left panels show net exchange-correlation potentials (solid line) and net exchange-correlation energy densities (dashed line). Right panels show corresponding pseudopotentials for $l=0$ (solid line), $l=1$ (dotted line), and $l=2$ (dashed line).

geometry for lattice constants 3.12 Å $\leq a \leq$ 3.17 Å. For Nb, calculations were performed assuming the bcc geometry for lattice constants 3.23 Å $\leq a \leq$ 3.31 Å. For both Nb and W, the maximum cohesive energy and the bulk modulus were determined by fitting the calculated energies to a quadratic function of a.

Table II lists the various contributions to the maximum cohesive energy for W for both the LDA form of the exchange-correlation interaction [using form (18a) for the core-cancellation function] and the GGA-II form of the exchange-correlation interaction [using form (18b) for the core-cancellation function]. From this table it is apparent that the atomic and Ewald energies are numerically the largest contributions, while E_{xc} is less than 5% of total electronic pseudoenergy of the solid.

The present results are compared with those of previ-

TABLE I. Calculational parameters.

	Nb	W
Pseudopotential radii ($l_{max}=2$):		
r_0	1.5 bohr	1.4 bohr
r_1	2.8	2.6
r_2	2.8	2.6
Cutoff radius for cancellation functions:		
r_c	2.8	2.6
Cutoff and convergence parameters for self-consistent band structure:		
Q_{max}	20 bohr^{-1}	20 bohr^{-1}
q_{PW}	4 bohr^{-1}	4 bohr^{-1}
q_{LCAO}	8 bohr^{-1}	8 bohr^{-1}
Δ_ρ	1×10^{-5} bohr^{-3}	1×10^{-5} bohr^{-3}
σ	0.1 eV	0.1 eV
Number of inequivalent **k** points for BZ sampling:		
	68	68

TABLE II. Contributions to the cohesive energy of W.

		LDA	GGA-II
Equilibrium lattice constant		$a=3.13$ Å	$a=3.15$ Å
Cohesive energy constributions	E_{atom}	−227.463 eV	−227.516 eV
	E_{Ewal}	−301.366	−299.452
	E_{one}	73.996	73.996
	E_{Coul}	−1.732	−1.755
	E_{xc}	−11.234	−11.467
	E_{ck}	0.107	0.094
	E_{coh}	12.765	11.068
	$\Delta E_{\text{atom}}^{\text{multi}}$	1.714	1.714
	$E_{\text{coh}}^{\text{corr}}$	11.05 eV	9.35 eV

ous workers in Table III. This comparison shows that the calculated results are sensitive to the computational details and to the form of the exchange-correlation functional. Körling and Häglund[35] performed calculations using both the LDA and GGA-II forms of the exchange-correlation functionals, but since they used the muffin-tin approximation, it is difficult to directly compare their results with the present work. García *et al.*[34] used mixed-basis pseudopotential techniques[13] and partial core corrections,[7] comparing the LDA functional with an earlier form of the generalized gradient approximation. The other results cited in Table III used the LDA with the Wigner[40] interpolation formula (Refs. 9, 31, 36, and 37), or with the Hedin-Lundqvist[41] or similar interpolation formula (Refs. 21, 38, and 39). Unlike the results of the present work, the cohesive energies listed in Table III were calculated relative to the spin polarized atomic calculations without using the experimental estimate for the multiplet splitting indicated in Eq. (14).

It seems to be well established[5] (although embarrass-

TABLE III. Comparison of ground-state cohesive properties for Nb and W.

	Lattice constant (Å)	Cohesive energy (eV/atom)	Bulk modulus (Mbar)
	Nb		
Experiment	3.30[a]	7.57[a]	1.70[b]
Present calculation (GGA-II)	3.28	8.15[c]	1.9
(LDA)	3.24	9.71[c]	1.9
Previous calculations:			
García *et al.* (GGA-I) (Ref. 34)	3.33	6.45	1.60
(LDA) (Ref. 34)	3.27	8.15	1.72
Körling and Häglund			
(GGA-II) (Ref. 35)	3.38		1.66
(LDA) (Ref. 35)	3.32		1.76
Fu and Ho (Ref. 21)	3.26	7.55	1.82
Harmon *et al.* (Ref. 36)	3.34	6.63	1.62
	W		
Experiment	3.16[a]	8.90[a]	3.10[b]
Present calculation (GGA-II)	3.15	9.35[d]	2.9
(LDA)	3.13	11.05[d]	2.9
Previous calculations:			
Körling and Häglund			
(GGA-II) (Ref. 35)	3.25		2.72
(LDA) (Ref. 35)	3.21		3.03
Mattheiss and Hamann (Ref. 37)	3.162	9.83	3.40
Wei *et al.* (Ref. 31)	3.164	10.09	3.18
Jansen and Freeman (Ref. 38)	3.149	9.76	3.46
Bylander and Kleinman (Ref. 9)	3.162	8.93	2.97
Zunger and Cohen (Ref. 39)	3.173	7.90	3.45

[a]Reference 32.
[b]Reference 33.
[c]Including multiplet correction $\Delta E_{\text{atom}}^{\text{mult}}=1.49$ eV.
[d]Including multiplet correction $\Delta E_{\text{atom}}^{\text{mult}}=1.71$ eV.

ing) that the LDA in the Wigner[40] form gives results for the equilibrium lattice constant in closest agreement with experiment, which accounts for its wide use.[9,31,36,37] However, using the "first-principles" LDA form of Ceperley and Alder[28] as parametrized by Perdew and Wang,[11] we find the LDA equilibrium lattice constants for Nb and W to be smaller than their experimental values by a few percent. In addition, even with atomic multiplet corrections, the LDA cohesive energies are larger than the experimental values by more than 2 eV. These systematic errors of the LDA have been noted by other workers.[42,43] These errors are partially corrected by the GGA-II as noted in Table III. For both Nb and W, the equilibrium lattice constants and the cohesive energies calculated with the GGA-II exchange-correlation functional are considerably closer to the experimental values than those calculated with the LDA form. The GGA-II correction to the cohesive energy can be partially understood as a correction to the treatment of the atomic ionization energies which are made possible by the Becke functional[44] which is included in the GGA-II formalism. However, the GGA-II must also correct some of the solid-state effects as evidenced by the improved agreement of the equilibrium lattice constants. Evidently, the GGA-II functional is also an improvement over earlier generalized gradient forms.[34] We find that the bulk modulus is very sensitive to the calculational details even with our highly converged calculations; both the LDA and GGA-II forms give very similar results for the bulk modulus.

Contour plots of the self-consistent valence pseudodensities generated using the GGA-II exchange-correlation form are shown in the top panels of Figs. 4 and 5 for Nb and W, respectively. Similar plots for pseudodensities generated using the LDA form are indistinguishable on this scale. These valence charge density contours are similar to results published by previous workers.[9,39,45] One would expect the difference between the GGA-II and LDA results for the cohesive energy to be reflected in the self-consistent valence densities. In the bottom panels of Figs. 4 and 5, the difference pseudodensities $\Delta\rho \equiv \rho^{\text{GGA-II}} - \rho^{\text{LDA}}$, magnified by a factor of $\times 100$, are plotted for Nb and W. The density differences are less than 1% of the valence pseudodensities themselves and have several regions of each sign. Some of the structure

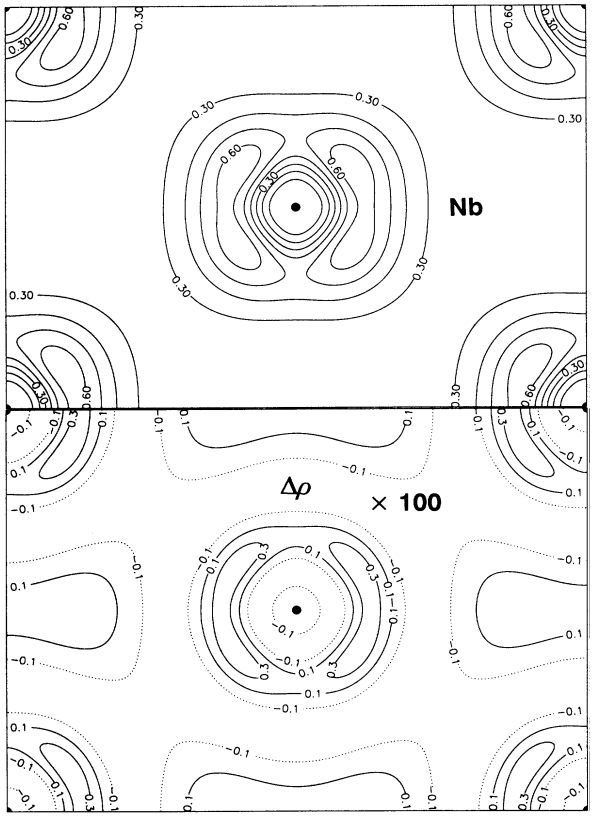

FIG. 4. Contour plot of the self-consistent valence-electron pseudodensity of Nb plotted in a (110) plane in units of electrons/Å^{-3} evaluated at lattice constant $a = 3.27$ Å. Upper panel shows valence electron density for the GGA-II calculation. Lower panel shows density difference $\Delta\rho \equiv \rho^{\text{GGA-II}} - \rho^{\text{LDA}}$ magnified 100 times. Positive contours are indicated with a full line, negative contours are indicated with a dotted line. Atomic positions are indicated with filled circles.

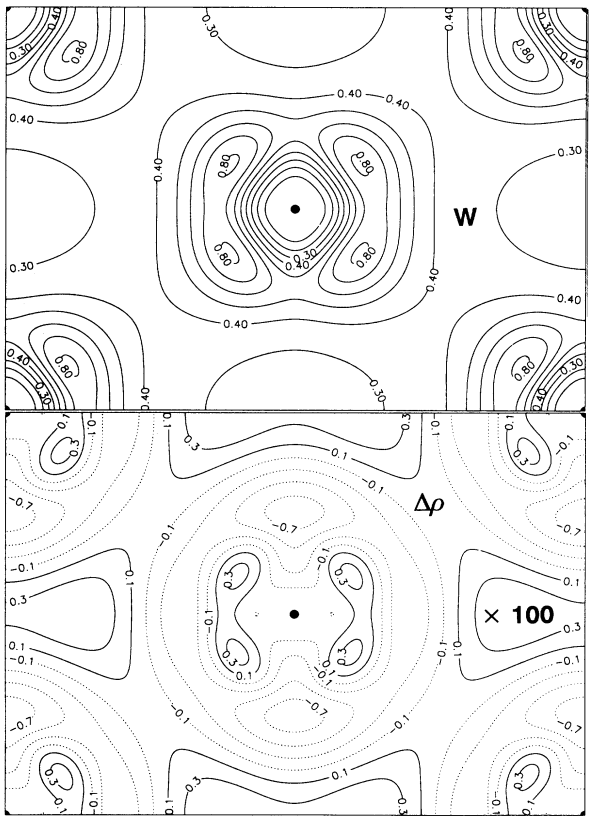

FIG. 5. Contour plot of the self-consistent valence-electron pseudodensity of W plotted in a (110) plane in units of electrons/Å^{-3} evaluated at lattice constant $a = 3.15$ Å. Upper panel shows valence electron density for the GGA-II calculation. Lower panel shows density difference $\Delta\rho \equiv \rho^{\text{GGA-II}} - \rho^{\text{LDA}}$ magnified 100 times. Positive contours are indicated with a full line, negative contours are indicated with a dotted line. Atomic positions are indicated with filled circles.

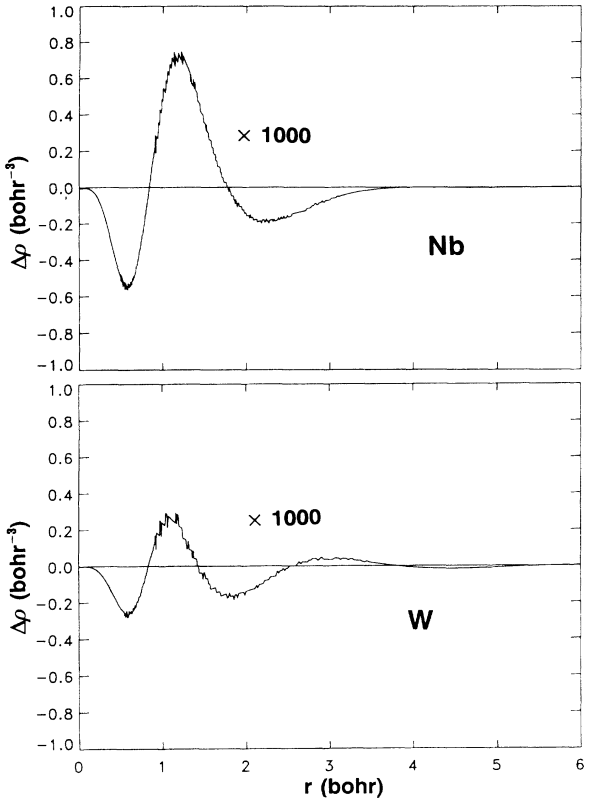

FIG. 6. Radial plot of the density difference $\Delta\rho \equiv \rho^{\text{GGA-II}} - \rho^{\text{LDA}}$ between the GGA-II and LDA pseudodensities for Nb and W atoms, magnified 1000 times.

of the difference densities is an atomic effect as evidenced in Fig. 6 which shows radial plots of the difference between the GGA-II and LDA atomic valence pseudodensities magnified by a factor $\times 1000$ for Nb (upper panel) and W (lower panel). The structure in the core region $0 \le r \le r_c$ is an artifact of the pseudopotential approximation, but the structure in the valence region $r > r_c$ is expected to represent the physical density difference. The bottom panels of Figs. 4 and 5 show that for both Nb and W, relative to the LDA valence density, the GGA-II valence density is slightly smaller in the nearest-neighbor bond region and slightly larger in the interstitial regions.

IV. SUMMARY AND CONCLUSIONS

In this paper we have described and demonstrated methods for improving the accuracy of first-principles electronic structure calculations within density-functional theory. In particular, we have introduced the core-cancellation functions, which provide an effective tool for efficient and accurate calculation of the exchange-correlation interactions, especially for materials involving transition metals. We find that when pushed to the limits of accuracy, the LDA form of the exchange-correlation interaction overestimates the cohesive energy of Nb and W by more than 2 eV and underestimates the equilibrium lattice constant by a few percent. The GGA-II form of the exchange-correlation interaction reduces the error in both the cohesive energy and the equilibrium lattice constant for both of these materials. On the basis of this study, we conclude that the GGA-II provides an improvement to the LDA description of the electronic structure of Nb and W. Further improvements in the exchange-correlation functional, as well as inclusion of other effects such as spin-orbit interaction and spin polarization effects, warrant further study.

The calculation methods described in this paper can be used for a wide variety of electronic structural studies. We have used it to study multilayer relaxation in W (111) thin films[46] and to study the transition metal compound materials FeS_2 and RuS_2.[47]

ACKNOWLEDGMENTS

We would like to thank J. Perdew for sending us a copy of his GGA-II subroutines and for clarifying some of our questions regarding their usage. We would also like to thank S. G. Louie and S. Fahy for helpful comments on the LDA overbinding problem. This work was supported by NSF Grant No. DMR-8918712 and by the North Carolina Supercomputer Center.

[1]P. Hohenberg and W. Kohn, Phys. Rev. **136**, B864 (1964); W. Kohn and L. J. Sham, Phys. Rev. **140**, A1133 (1965).
[2]James F. Annett, Phys. Rev. Lett. **69**, 2244 (1992).
[3]D. M. Bylander and Leonard Kleinman, Phys. Rev. B **43**, 12 070 (1991).
[4]E. L. Shirley, R. M. Martin, and G. B. Bachelet, Phys. Rev. B **42**, 5057 (1990); F. R. Vukajlovic, E. L. Shirley, and R. M. Martin, *ibid.* **43**, 3994 (1991).
[5]W. E. Pickett, Comput. Phys. Rep. **9**, 115 (1989).
[6]M. C. Payne, M. P. Teter, D. C. Allan, T. A. Arias, and J. D. Joannopoulos, Rev. Mod. Phys. **64**, 1045 (1992).
[7]S. G. Louie, S. Froyen, and M. L. Cohen, Phys. Rev. B **26**, 1738 (1982).
[8]J. Zhu, X. W. Wang, and S. G. Louie, Phys. Rev. B **45**, 8887 (1992).
[9]D. M. Bylander and L. Kleinman, Phys. Rev. B **27**, 3152 (1983).
[10]J. R. Gardner and N. A. W. Holzwarth, Phys. Rev. B **33**, 7139 (1986).
[11]J. P. Perdew and Y. Wang, Phys. Rev. B **45**, 13 244 (1992).
[12]J. P. Perdew, J. A. Chevary, S. H. Vosko, K. A. Jackson, M. R. Pederson, D. J. Singh, and C. Fiolhais, Phys. Rev. B **46**, 6671 (1992).
[13]S. G. Louie, K.-M. Ho, and M. L. Cohen, Phys. Rev. B **19**, 1774 (1979).
[14]L. Kleinman, Phys. Rev. B **21**, 2630 (1980).
[15]G. B. Bachelet, D. R. Hamann, and M. Schlüter, Phys. Rev. B **26**, 4199 (1982).
[16]G. P. Kerker, J. Phys. C **13**, L189 (1980).
[17]N. Troullier and J. L. Martins, Phys. Rev. B **43**, 1993 (1991).
[18]The separable form used in the present work was based on orthogonal polynomials constructed within the core sphere.
[19]B. T. Smith, J. M. Boyle, J. J. Dongarra, B. S. Garbow, Y. Ikebe, V. C. Klema, and C. B. Moler, *Matrix Eigensystems Routines-EISPACK Guide* (Springer-Verlag, Berlin, 1976).
[20]G. Gilat and Z. Kam, Phys. Rev. Lett. **22**, 715 (1969).

[21]C.-L. Fu and K.-M. Ho, Phys. Rev. B **28**, 5480 (1983).
[22]C. G. Broyden, Math. Comput. **19**, 577 (1965).
[23]G. P. Srivastava, J. Phys. A **17**, L317 (1984); Note: there is a sign error in Eqs. 16 of this reference.
[24]P. P. Ewald, Ann. Phys. (Leipzig) **64**, 253 (1921).
[25]J. Ihm, A. Zunger, and M. L. Cohen, J. Phys. C **12**, 4409 (1979); **13**, 3095 (1980); J. Ihm, Rep. Prog. Phys. **51**, 105 (1988).
[26]Charlotte E. Moore, *Atomic Energy Levels,* Nat. Stand. Ref. Data Ser., Nat. Bur. Stand. (U.S.), NSRDS-NBS 35, SD Catalog No. C13.48:35 (U.S. GPO, Washington, D.C., 1971), Vol. I-III.
[27]G. W. Fernando, R. E. Watson, M. Weinert, Y. J. Wang, and J. W. Davenport, Phys. Rev. B **41**, 11 813 (1990).
[28]D. M. Ceperley and B. J. Alder, Phys. Rev. Lett. **45**, 566 (1980).
[29]A. H. MacDonald and S. H. Vosko, J. Phys. C **12**, 2977 (1979).
[30]A. K. Rajagopal, J. Phys. C **11**, L943 (1978).
[31]S.-H. Wei, H. Krakauer, and M. Weinert, Phys. Rev. B **32**, 7792 (1985).
[32]Charles Kittel, *Introduction to Solid State Physics,* 6th ed. (Wiley, New York, 1986).
[33]A. Fernández Guillermet and G. Grimvall, Phys. Rev. B **40**, 1521 (1989).
[34]A. García, C. Elsässer, J. Zhu, S. G. Louie, and M. L. Cohen, Phys. Rev. B **46**, 9829 (1992); **47**, 4150(E) (1993). The values quoted in Table III as "GGA-I" correspond to the result labeled BP for both the core and valence densities.
[35]M. Körling and J. Häglund, Phys. Rev. B **45**, 13 293 (1992). The cohesive energies were included in this paper in graphical form.
[36]B. N. Harmon, W. Weber, and D. R. Hamann, J. Phys. Colloq. **C6**, 628 (1981).
[37]L. F. Mattheiss and D. R. Hamann, Phys. Rev. B **33**, 823 (1986).
[38]H. J. F. Jansen and A. J. Freeman, Phys. Rev. B **30**, 561 (1984).
[39]A. Zunger and M. L. Cohen, Phys. Rev. B **19**, 568 (1979).
[40]E. Wigner, Phys. Rev. **46**, 1002 (1934).
[41]L. Hedin and B. I. Lundqvist, J. Phys. C **4**, 2064 (1971).
[42]R. E. Watson, G. W. Fernando, M. Weinert, Y. J. Wang, and J. W. Davenport, Phys. Rev. B **43**, 1455 (1991).
[43]S. Fahy, X. W. Wang, and S. G. Louie, Phys. Rev. B **42**, 3503 (1990).
[44]A. D. Becke, Phys. Rev. A **38**, 3098 (1988).
[45]K.-M. Ho, S. G. Louie, J. R. Chelikowsky, and M. L. Cohen, Phys. Rev. B **15**, 1755 (1977).
[46]N. A. W. Holzwarth, J. A. Chervenak, C. J. Kimmer, Y. Zeng, W. Xu, and J. Adams, Phys. Rev. B **48**, 12 136 (1993).
[47]Y. Zeng and N. A. W. Holzwarth (unpublished).